REPORT DOCUMENTATION PAGE

Form Approved OMB NO. 0704-0188

1. REPORT DATE (DD-MM-YYYY)	2. REPORT TYPE	3. DATES COVERED (From - To)
31-12-2007	Final Report	4-Jun-2003 - 3-Jun-2007

4. TITLE AND SUBTITLE
Investigation of Quantum Computing with Laughlin Quasiparticles

5a. CONTRACT NUMBER
DAAD19-03-1-0126

5b. GRANT NUMBER

5c. PROGRAM ELEMENT NUMBER

6. AUTHORS
V. J. Goldman

5d. PROJECT NUMBER

5e. TASK NUMBER

5f. WORK UNIT NUMBER

7. PERFORMING ORGANIZATION NAMES AND ADDRESSES
State University of New York at Stony Brook
Office of Sponsored Programs
Research Foundation Of SUNY
Stony Brook, NY 11794 -3362

8. PERFORMING ORGANIZATION REPORT NUMBER

9. SPONSORING/MONITORING AGENCY NAME(S) AND ADDRESS(ES)
U.S. Army Research Office
P.O. Box 12211
Research Triangle Park, NC 27709-2211

10. SPONSOR/MONITOR'S ACRONYM(S)
ARO

11. SPONSOR/MONITOR'S REPORT NUMBER(S)
44999-PH-QC.1

12. DISTRIBUTION AVAILIBILITY STATEMENT
Approved for public release; Federal purpose rights

13. SUPPLEMENTARY NOTES
The views, opinions and/or findings contained in this report are those of the author(s) and should not contrued as an official Department of the Army position, policy or decision, unless so designated by other documentation.

14. ABSTRACT
Laughlin quasiparticles of a gapped fractional quantum Hall (FQH) fluid, have been demonstrated to have fractional electric charge and anyonic braiding statistics. Topological computation with anyons has been proposed as the physical implementation of intrinsically fault-tolerant quantum computation (QC). Topological computation employs the statistical Berry phase created by the transfer of one anyon of the system around another to perform quantum logic. Since this phase is determined by the topological properties of the macroscopic FQH wave function, it is not sensitive to environment-induced decoherence and to spread of device parameters. The most thoroughly studied and realistic proposals involve the ground

15. SUBJECT TERMS
quantum computation

16. SECURITY CLASSIFICATION OF:			17. LIMITATION OF ABSTRACT	15. NUMBER OF PAGES	19a. NAME OF RESPONSIBLE PERSON
a. REPORT	b. ABSTRACT	c. THIS PAGE			Vladimir Goldman
U	U	U	SAR		19b. TELEPHONE NUMBER: 631-632-9001

Report Title

Investigation of Quantum Computing with Laughlin Quasiparticles

ABSTRACT

Laughlin quasiparticles of a gapped fractional quantum Hall (FQH) fluid, have been demonstrated to have fractional electric charge and anyonic braiding statistics. Topological computation with anyons has been proposed as the physical implementation of intrinsically fault-tolerant quantum computation (QC). Topological computation employs the statistical Berry phase created by the transfer of one anyon of the system around another to perform quantum logic. Since this phase is determined by the topological properties of the macroscopic FQH wave function, it is not sensitive to environment-induced decoherence and to spread of device parameters. The most thoroughly studied and realistic proposals involve the ground state adiabatic transport of anyons localized on quantum antidots and in anyon interferometers defined in GaAs/AlGaAs heterostructures. The device fabrication techniques and 2D architectures are similar to those commonly used in semiconductor industry, and thus are inherently scalable.

List of papers submitted or published that acknowledge ARO support during this reporting period. List the papers, including journal references, in the following categories:

(a) Papers published in peer-reviewed journals (N/A for none)

V. V. Ponomarenko and D. V. Averin, Strong-coupling branching between edges of fractional quantum Hall liquids, Phys. Rev. B 70,195316 (2004).

V. V. Ponomarenko and D. V. Averin, Antidot tunneling between quantum Hall liquids with different filling factors, Phys. Rev. B 71, 241308 (2005).

Fractional statistics of Laughlin quasiparticles in quantum antidots
Physical Review B 71, 153303, 1-3 (2005)
V.J.Goldman, J.Liu, and A.Zaslavsky

Realization of a Laughlin quasiparticle interferometer: Observation of fractional statistics
Physical Review B 72, 075342, 1-8 (2005)
F.E.Camino, W.Zhou, and V.J.Goldman

Aharonov-Bohm electron interferometer in the integer quantum Hall regime
Physical Review B 72, 155313, 1-6 (2005)
F.E.Camino, W.Zhou, and V.J.Goldman

Aharonov-Bohm Superperiod in a Laughlin Quasiparticle Interferometer
Physical Review Letters 95, 246802, 1-4 (2005)
F.E.Camino, W.Zhou, and V.J.Goldman

Flux period scaling in the Laughlin quasiparticle interferometer
Physical Review B 73, 245322, 1-5 (2006)
W.Zhou, F.E.Camino, and V.J.Goldman

Transport in the Laughlin quasiparticle interferometer: Evidence for topological protection in an anyonic qubit
Physical Review B 74, 115301, 1-8 (2006)
F.E.Camino, W.Zhou, and V.J.Goldman

Superperiods and quantum statistics of Laughlin quasiparticles
Physical Review B 75, 045334, 1-11 (2007)
V.J.Goldman

e/3 Laughlin Quasiparticle Primary-Filling nu = 1/3 Interferometer
Physical Review Letters 98, 076805, 1-4 (2007)
F.E.Camino, W.Zhou, and V.J.Goldman

Mach-Zehnder Interferometer in the Fractional Quantum Hall Regime
Phys. Rev. Lett. 99, 066803 (2007)
V.V.Ponomarenko and D.V.Averin

Coulomb Blockade of Anyons in Quantum Antidots
D.V.Averin and J.A.Nesteroff
Phys. Rev. Lett. 99, 096801 (2007)

Quantum transport in electron Fabry-Perot interferometers
Physical Review B 76, 155305, 1-6 (2007)
F.E.Camino, W.Zhou, and V.J.Goldman

Number of Papers published in peer-reviewed journals: 14.00

(b) Papers published in non-peer-reviewed journals or in conference proceedings (N/A for none)

Fractional quantum Hall effect: A game of five halves (News and Views)
Nature Physics 3, 517 - 518 (2007)
V.J.Goldman

Number of Papers published in non peer-reviewed journals: 1.00

(c) Presentations

Number of Presentations: 0.00

Non Peer-Reviewed Conference Proceeding publications (other than abstracts):

Number of Non Peer-Reviewed Conference Proceeding publications (other than abstracts): 0

Peer-Reviewed Conference Proceeding publications (other than abstracts):

Number of Peer-Reviewed Conference Proceeding publications (other than abstracts): 0

(d) Manuscripts

Number of Manuscripts: 0.00

Number of Inventions:

Graduate Students

NAME	PERCENT_SUPPORTED
Wei Zhou	0.80
James Nesteroff	1.00
FTE Equivalent:	**1.80**
Total Number:	**2**

Names of Post Doctorates

NAME	PERCENT_SUPPORTED
Fernando Camino	0.75
Vadim Ponomarenko	1.00
FTE Equivalent:	**1.75**
Total Number:	**2**

Names of Faculty Supported

NAME	PERCENT_SUPPORTED	National Academy Member
Vladimir J. Goldman	0.03	No
Dmitri V. Averin	0.20	No
FTE Equivalent:	**0.23**	
Total Number:	**2**	

Names of Under Graduate students supported

NAME	PERCENT_SUPPORTED
FTE Equivalent:	
Total Number:	

Student Metrics

This section only applies to graduating undergraduates supported by this agreement in this reporting period

The number of undergraduates funded by this agreement who graduated during this period:	0.00
The number of undergraduates funded by this agreement who graduated during this period with a degree in science, mathematics, engineering, or technology fields:.....	0.00
The number of undergraduates funded by your agreement who graduated during this period and will continue to pursue a graduate or Ph.D. degree in science, mathematics, engineering, or technology fields:.....	0.00
Number of graduating undergraduates who achieved a 3.5 GPA to 4.0 (4.0 max scale):	0.00
Number of graduating undergraduates funded by a DoD funded Center of Excellence grant for Education, Research and Engineering:	0.00
The number of undergraduates funded by your agreement who graduated during this period and intend to work for the Department of Defense	0.00
The number of undergraduates funded by your agreement who graduated during this period and will receive scholarships or fellowships for further studies in science, mathematics, engineering or technology fields:	0.00

Names of Personnel receiving masters degrees

NAME
james nesteroff
Total Number: 1

Names of personnel receiving PHDs

NAME
Wei Zhou
Total Number: 1

Names of other research staff

NAME	PERCENT_SUPPORTED
none	No
FTE Equivalent:	
Total Number: 1	

Sub Contractors (DD882)

Inventions (DD882)

Scientific progress under ARO support

In the first half of this funding period, we have spent considerable time and effort to develop new kinds of samples (the LQP interferometers and lithographic double-antidot qubits), to learn to experimentally control them, and to understand what's going on in these devices. During this time there was little publishable results. Once developed, however, these samples have yielded (and continue to yield) a good deal of new results, both in the integer and, especially, in the FQH regimes. Several key experimental barriers have been removed, and the theoretical basis of the topological quantum computation has received experimentally-demonstrated foundation. In particular, we demonstrated fractional braiding statistical phase of LQP's, robustness of this topological phase as a function of temperature and its insensitivity to control front gate bias. We also fabricated lithographic double-QAD qubits and demonstrated coherent LQP transport in these devices. Theoretical work elucidated how to separate the enclosed flux and statistical contributions in QAD transport and developed chiral Luttinger Liquid techniques for analysis of the LQP tunneling dynamics in the QAD qubit. These significant advances have laid foundation for this proposal.

2.1. *Statistics of Laughlin quasiparticles in quantum antidots*. -- A quantum antidot electrometer has been used in the first direct observation of the charge *e*/3 and *e*/5 quasiparticles. [12,13] The wave functions of a charge *q* particle encircling the antidot are quantized by the condition that the Berry phase of the *m*-th orbital $\gamma_m = q\Phi/\hbar + 2\pi\Theta N = 2\pi m$, where *m* is an integer, Φ is the enclosed flux and *N* is the number of particles being encircled. This quantization condition explicitly adds the Aharonov-Bohm and the statistical contributions to the total Berry phase. In experiments, the occupation of the antidot-bound LQP orbitals is monitored by the inter-edge two-step resonant tunneling. Each step is a phase-coherent tunneling between two many-body configurations: one in which a LQP is localized on an extended edge, and one in which it is localized on the antidot. A peak of the tunneling conductance is thus observed when an antidot-bound LQP state crosses μ, the orbital quantum number $m \to m+1$, and the phase period is $\Delta_\gamma = 2\pi$. The two different ways to shift the orbitals relative to μ are: (i) to vary the applied magnetic field, in a kind of the Aharonov-Bohm effect giving the flux period Δ_Φ, and (ii) to vary the global backgate voltage, which produces an electric field normal to the 2D electron layer and allows to measure the LQP electric charge, Fig. 1(a). The flux period of a particle of charge *q* in vacuum is $\Delta_\Phi = 2\pi\hbar/q$. Thus, if a charge *e*/3 particle existed in vacuum, its flux period would be 3*h*/*e*. However, the *e*/3 Laughlin quasiparticle encircling the antidot does not exist in vacuum, and thus the statistical contribution from the enclosed particles must be taken into account. Thus, the experimental $\Delta_{\Phi_{1/3}} = h/e$ yields quasihole braiding statistics $\Theta_{1/3} = 2/3$, Fig. 1(b). [18]

2.2. *Experimental demonstration of anyonic braiding statistics.* -- We have realized a novel Laughlin quasiparticle interferometer, where, for the first time, we have observed an Aharonov-Bohm (A-B) "superperiod" implying fractional statistics of quasiparticles. [14,15,21] We have developed novel 2D electron interferometer samples in low-density, high mobility AlGaAs/GaAs heterojunction material using electron beam lithographic techniques. In these samples, 2D electrons (230 - 300 nm below the GaAs surface) are prepared by exposure to red light at 4.2 K. The four independently-contacted front gates were defined by electron beam lithography on a pre-etched mesa with Ohmic contacts. After a shallow 140 nm wet chemical etching, the 50 nm thick Au/Ti gate metal was deposited in etch trenches, followed a self-aligned lift-off process, see Fig. 3(a, b). The etch trenches define an approximately circular 2D electron island of lithographic radius $R = 600\ldots3{,}000$ nm. The need to define narrow and long front gate leads, separated by 300 - 500 nm wide, ~150 μm long insulating gap by electron beam lithography required use of proximity correction. In the QH regime of interest here, it is important to have gap between the gates totally

depleted of electrons, even at zero or even positive front gate voltage, yet the gap must survive intentional or accidental application of a 5 V differential bias between the neighboring gates. It is also nontrivial to run the narrow gate metal leads up the optical mesa wall without loss of electrical continuity. The back gate technique developed previously for quantum antidot samples was adapted without major modifications.

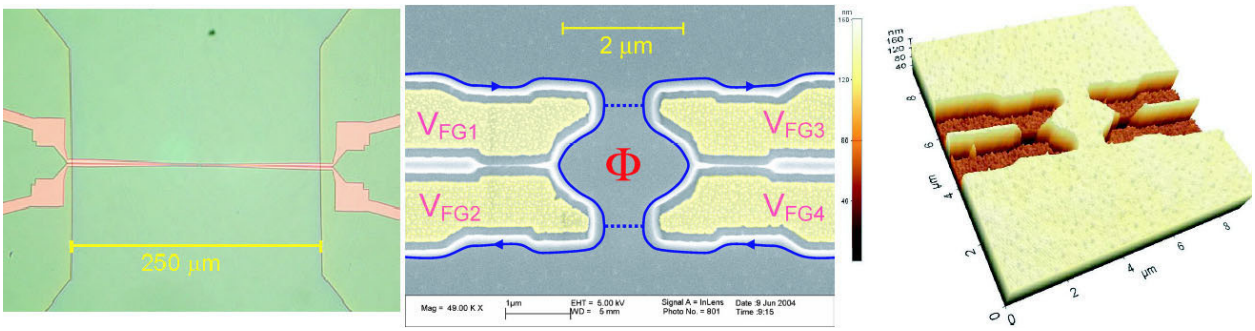

Fig. 3. Optical, SEM, and AFM micrographs (from left to right) of an electron interferometer sample. The constrictions are 1,100 nm wide. Four Ohmic contacts (not shown) are positioned at the corners of a 4×4 mm sample. On a QH plateau, current flows along the counterpropagating chiral edge channels (blue lines). Tunneling (represented by dots) occurs in the two wide constrictions, when the edge channels are close enough, thus allowing the electrons to perform a closed path around the 2DES island. The Aharonov-Bohm interference signal is detected as oscillations in R_{xx}.

The depletion potential has a saddle point in the constrictions, and so has the resulting electron density profile, see Fig. 4. In a quantizing B, the tunneling between the chiral edge channels (possible only over a few magnetic lengths $\ell = \sqrt{\hbar / eB}$) occurs near the saddle points. Thus, when A-B oscillations are observed, the island edge channel filling is determined by the saddle point filling. The saddle point density in the constrictions can be determined experimentally from magnetotransport data. We varied the lithographic parameters to achieve $n_C \approx 0.75 n_B$, which is essential in order to achieve a regime when $f = 1/3$ in the constrictions while $f = 2/5$ in the island center [in a given B, $\nu \propto n$, and (1/3)/(2/5)=0.833]. Confinement of 2D electrons by the etched trenches is much more sharp than by the means of negatively biased front gates alone, see Fig. 4(a) (note that 2DES is completely depleted for $R - W < r < R$). Asymptotically, in large islands, $n(r)$ heals as $r^{-3/2}$ for confinement [22] by the etch trenches versus only $r^{-1/2}$ for front gates. [23] The gradient of the self-consistent confining potential (including the screening by the 2D electrons of the bare potential) is approximately proportional to $-e(\partial n / \partial r)$, so the confinement by the etched trenches results in a better-defined island radius, greater edge velocity, and also the island center density n_I much

closer (within a few %) to the bulk n_B, compared with confinement by gates alone. In addition, the constriction n_C can be controlled much better, without much effect on the island center density.

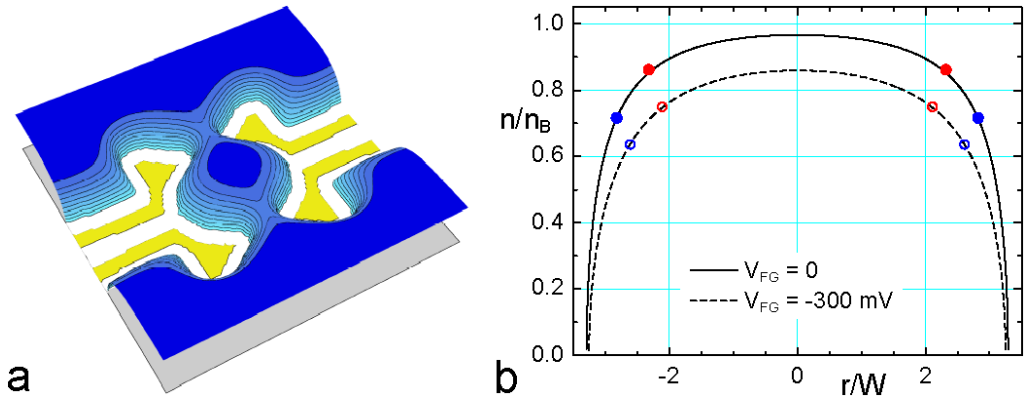

Fig. 4. (a) A qualitative illustration of the 2D electron density n profile. (b) The calculated electron density profile $n(r)$ in a circular island defined by an etched annulus of inner radius $R \approx 1{,}050$ nm, $n_B = 1.2\times10^{11}$ cm^{-2}. The calculation follows the $B = 0$ model of Ref. 24. $W = 245$ nm is the depletion length parameter. The blue circles give the radius of the outer edge ring $r_{Out} \approx 685$ nm, obtained from the integer Aharonov-Bohm period and $n(r_{Out})$ from the B-field position on the constriction QH plateaus. The red circles give the inner edge ring radius $r_{In} \approx 570$ nm, obtained with the fractional $N_\Phi = 5$ and the density ratio $n(r_{In})/n(r_{Out}) = (2/5)/(1/3) = 1.20$. From [25].

In the FQH regime, we focus on the situation when an $f = 1/3$ annulus surrounds an island of the $f = 2/5$ FQH fluid, Fig. 5(b). Here, we observe A-B oscillations with period $\Delta_B = 20.1$ mT, see Fig. 5(c). Fig. 5(d) shows the analogous oscillations observed as a function of V_{BG}, with period $\Delta_V = 937$ mV. The oscillation period in this regime gives the *inner* edge ring radius of 570 nm. We can be confident that current must flow through an 1/3 region separating the two 2D bulk 2/5 regions with Ohmic contacts because the Hall resistance in this B-range is quantized to $R_{xy} = 3h/e^2$ (Fig. 1 of [26]). The ratio of the periods $\Delta_B/\Delta_V \propto N_\Phi/N_e = 1/f$ is independent of the edge ring area and thus can be used to establish the QH filling f originating the A-B oscillations. N_Φ and N_e are the number of flux quanta and electrons, respectively, within the area of the A-B path. The fact that the ratios fall on a straight line forced through zero and the integers 1 and 2 (Fig. 4 of [15]), confirms the island filling as $f = 2/5$ at $B \approx 11.9$ T.

We have reported experiments on flux period scaling in the electron interferometer devices in the quantum Hall regime. [25] We determined the dependence of the Aharonov-Bohm field period Δ_B on the front gate voltage V_{FG} for electrons ($f = 1$) and for Laughlin quasiparticles (2/5 embedded in 1/3). For moderate V_{FG} we find an

approximately linear dependence $d\Delta_B / dV_{FG} = const$ on each QH plateau. The directly measured Δ_B and the slope $d\Delta_B / dV_{FG}$, and the assumed S can be combined to give $V_{FG}(1e)$, the front gate voltage attracting charge $1e$ to the area of the A-B orbit [27]. Capacitance is defined as $C \equiv Q/V = e/V_{FG}(1e)$. For a 2D disc of radius r, the classical capacitance is approximately proportional to r, neglecting a slowly varying logarithmic term. For a large (~2000 electrons) 2D island, the quantum corrections to the classical capacitance are small, and the product $rV_{FG}(1e)$ should be approximately constant, independent of the QH filling or the area. Thus, equating the product $rV_{FG}(1e)$ for different QH regimes, the $f = 2/5$ island area $S = \pi r^2$ can be determined directly with a 10% accuracy. This is quite sufficient to distinguish the physically realistic possibilities of the flux periods $\Delta_\Phi = 5h/e$ [14,15], $5h/2e$ [28], h/e and $h/2e$ [29].

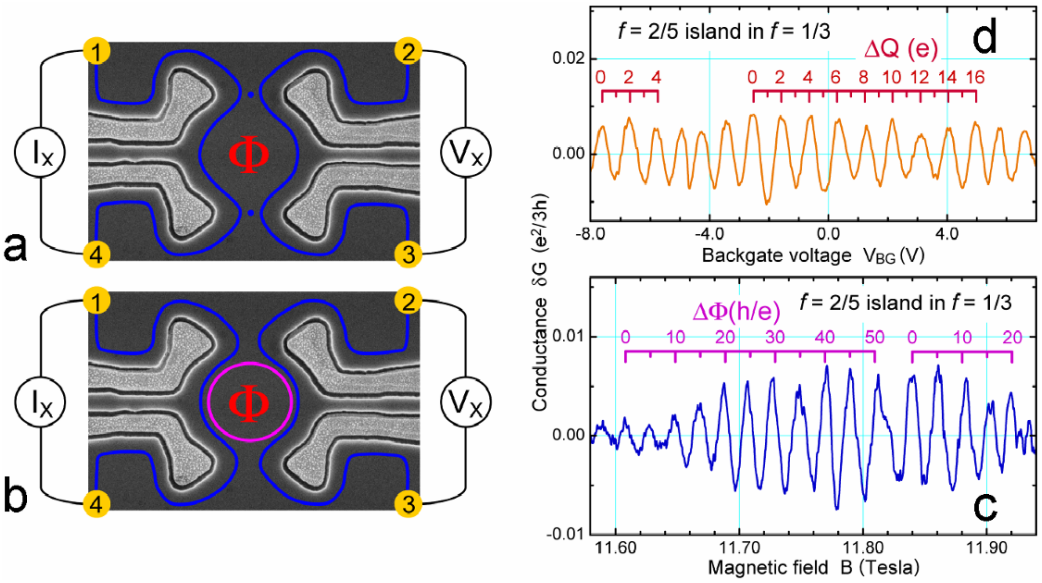

Fig. 5. (a,b) SEM of an interferometer sample with chiral edge channels superimposed. (a) In the IQH regime only one filling is present because $n_B/n_C \approx 1.3$, less than 2/1, e.g. (b) An inner $f = 2/5$ edge channel (pink) forms within the outer $f = 1/3$ channel (blue) that transports the current. The two are separated by ~15ℓ, and thus are coupled by tunneling. [30] (c,d) A-B interference of $e/3$ LQP's circling the 2/5 island. (c) Flux through the island period $\Delta_\Phi = 5h/e$ corresponds to creation of ten $e/5$ LQPs in the island [one h/e excites two $e/5$ LQPs from the 2/5 FQH condensate, the total (LQP's + FQH condensate) charge is fixed]. Such "superperiod" $\Delta_\Phi > h/e$ has never been reported before. (d) The backgate voltage period of $\Delta_Q = 2e = 10(e/5)$ directly confirms that the $e/3$ LQP consecutive orbits around the island are quantized by the condition requiring incremental addition of ten $e/5$ LQP's of the 2/5 fluid. From [14,15].

The striking feature of the conductance oscillations in Fig. 5(c) is the A-B period of five fundamental flux quanta: $\Delta_\Phi = 5h/e$! Such superperiod of $\Delta_\Phi > h/e$ has never been reported before. Addition of flux h/e to an area occupied by the 1/3 FQH condensate creates a vortex, an $e/3$ quasihole. [8] Likewise, addition of flux h/e to the 2/5 FQH fluid creates two vortices, that is, two $e/5$ quasiholes. These predictions have been verified at a microscopic level in the quantum antidot experiments. [12,13] Thus, addition of $5h/e$ to the 2/5 island creates ten $e/5$ LQPs with total charge $\Delta_Q = 2e$, in agreement with the backgate data in Fig. 5(d). In contrast, the periods observed in QADs correspond to addition of one LQP only, both for the 1/3 and 2/5 cases. The principal difference between the LQP interferometer and the QADs is that in QADs the FQH fluid surrounds electron vacuum, while in the LQP interferometer the 1/3 fluid surrounds an island of the 2/5 fluid. The gauge invariance argument [31,32] requiring $\Delta_\Phi \le h/e$ for the true A-B geometry is not applicable here because the interior of the edge ring contains electrons.

This A-B "superperiod" must be imposed by the symmetry properties of the two FQH fluids. The braiding statistics Θ of quasiparticles is analyzed as the Berry phase γ, analogous to the antidot treatment above. The $\Delta_\gamma = 2\pi$ period then contains two contributions: change of magnetic flux enclosed by the e/3 LQP orbits, and the statistics term taking into account that the number of the encircled $e/5$ quasiholes is changed by ten. The current used to measure conductance is transported by the quasiholes of the outside 1/3 fluid; therefore, we must construe that the conductance oscillations periodicity results from the 2π periodicity of the Berry phase γ of the $q = -e/3$ LQP encircling ten $e/5$ QP's of the $f = 2/5$ island:

$$\Delta\gamma = \frac{q}{\hbar}\Delta_\Phi + 2\pi\Delta_N\Theta = 2\pi[\frac{e}{3h}\frac{5h}{e} + 10\ \Theta_{2/5}^{1/3}] = 2\pi\ . \qquad (1)$$

This gives the relative statistics $\Theta_{2/5}^{-1/3} = 4/15$ between the 1/3 and the 2/5 FQH LQPs. [14,15]

The temperature T-dependence data show the $\Delta_\Phi = 5h/e$ A-B oscillations persisting to 140 mK. [26] Experiments show thermal dephasing of the Aharonov-Bohm oscillations in the novel LQP interferometer, where quasiparticles of the 1/3 FQH fluid execute a closed path around an island of the 2/5 fluid. Qualitatively, the experimental results follow a thermal dephasing dependence expected for an electron interferometer, the A-B amplitude to agree with the expected $\propto T/T_0 \sinh(T/T_0)$. This is in stark contrast to the $\propto 1/T\cosh(\Delta E/kT)$ observed in quantum antidots, the data is clearly different from the activated behavior observed in resonant tunneling and Coulomb blockade devices,

both in the chiral Luttinger Liquid (χLL) and the Fermi liquid regimes. [33,34] The data fit very well the χLL dependence predicted for a two point-contact LQP interferometer. [35] At the lowest experimental $T \leq 20$ mK, the small deviation from the zero-bias theoretical χLL dependence can be fit extremely well by including a finite bias, improving the overall fit. However, the value of the bias obtained in the fit is three times higher than the total of the known experimental sources, perhaps pointing to yet unrecognized source of experimental decoherence not included in theory. [26]

2.3. *Lithographic double-QAD qubits.* -- Qubit devices based on lithographic double quantum antidots have been fabricated, see Fig. 6, where we observed coherently-split tunneling peaks in the FQH regime. [20] These work required development of lithographic techniques for novel device fabrication, and the techniques and the expertise developed will be applied to the future work. Representative experimental transport and tunneling data is shown in Figs. 7 and 8. We encountered the not fully anticipated control problem of using only two front gates to tune for symmetry both: tunneling rates to electrode edges Γ_0 and Γ_1, and the bare (uncoupled) energies E_0 and E_1, see Fig. 2. It is believed that this problem was made worse by the cautious choice of the design inter-QAD separation of 560 nm, so as to ensure avoidance of the merging of the two QAD's into one. This resulted in a too small inter-QAD coupling Ω, to compensate which we had to reduce the 2DES density by ~2.5, from the preferred value (in Fig. 7, f = 1/3 FQH plateau is at $B \approx 4.5$ T, while desired working B ~12 T). An improved design qubit device with smaller QAD separation has been fabricated and is ready for low temperature characterization.

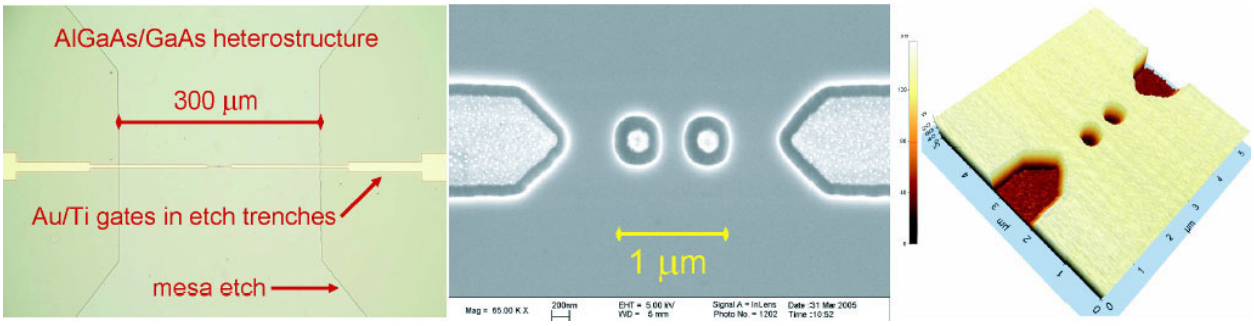

Fig. 6. Optical, SEM, and AFM micrographs (from left to right) of a double QAD qubit device fabricated in high-mobility, low-density 2DES GaAs/AlGaAs heterostructure. The 2D electron confinement potential is created by the etched trenches, the Au/Ti gates are deposited by a self-aligned lithography. The antidots are 180 nm diameter. Ohmic contacts (not shown) are positioned at the outside edge of a 4×4 mm mesa.

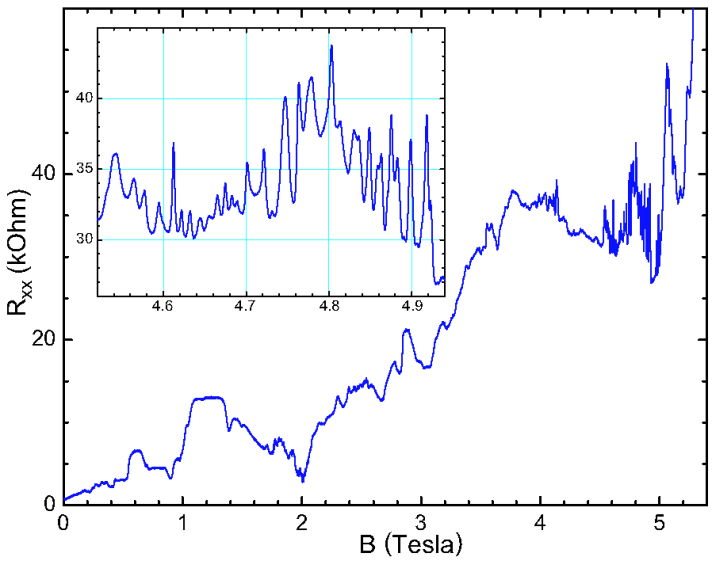

Fig. 7. Electron transport in a double-QAD qubit at 10.2 mK. The inset shows the LQP tunneling peaks on the $f = 1/3$ QH plateau. The tunneling signal is detected as peaks in R_{xx}. In this device, lithographic QAD separation of 560 nm is larger than optimal, reducing the QAD tunnel coupling. Observation of coherently-split peaks required a low 2D density, thus shifting the QH plateaus to inconveniently low B-field range. [20]

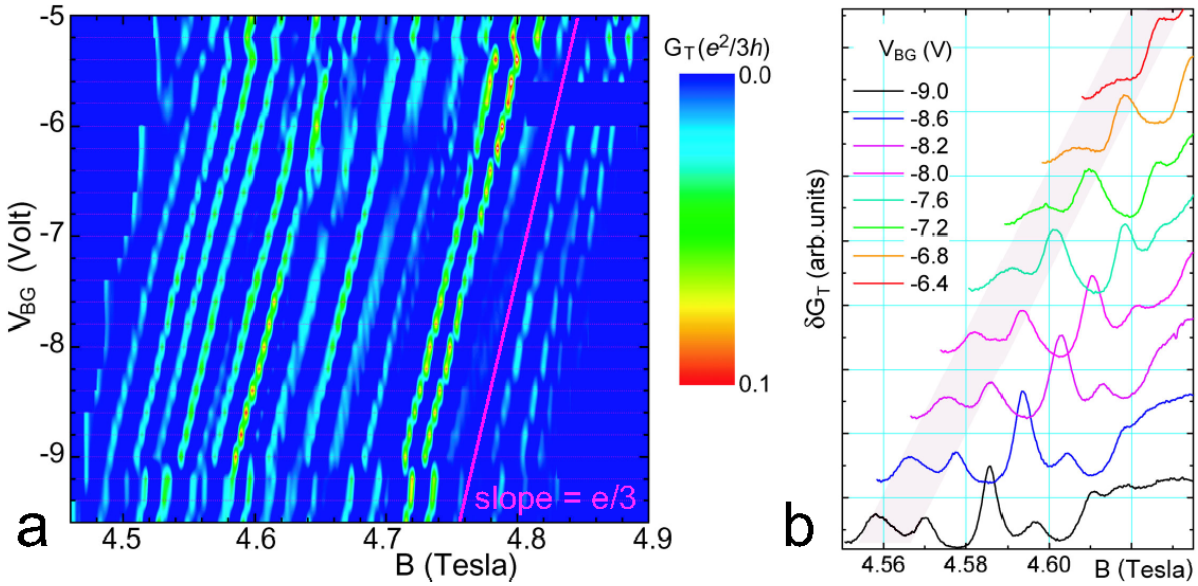

Fig. 8. Experimental tunneling conductance in QAD qubit in the $f = 1/3$ FQH fluid at 10.2 mK. (a) 3D contour plot of G_T vs. magnetic field and the back gate voltage V_{BG}. The slope of the G_T peaks in these coordinates gives the charge $e/3$ of the tunneling Laughlin quasiparticles. (b) Typical coherently-split G_T peaks. The shading traces the evolution of one coherently-split peak vs. back gate V_{BG}. Application of V_{BG} mostly affects Γ_0 and Γ_1, and thus their ratio, but not the splitting δ, in these data. [20]

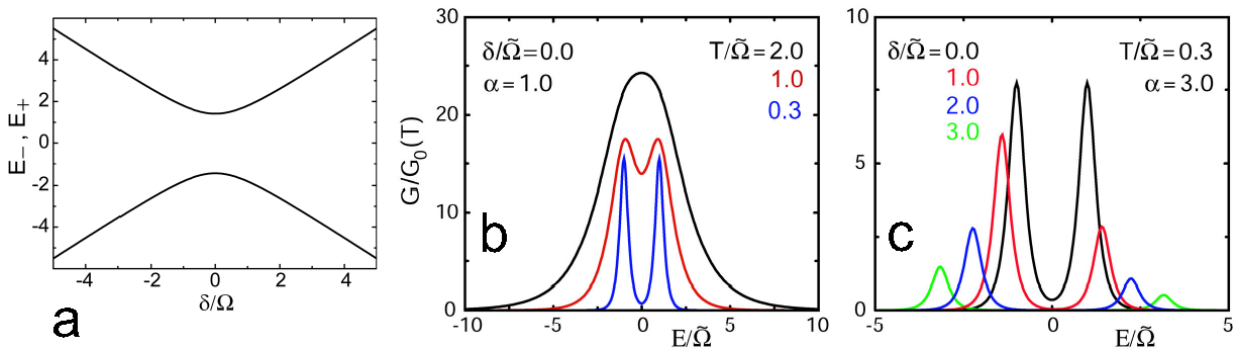

Fig. 9. (a) Symmetric/antisymmetric energies $E_{\pm}$ (in units of Ω) for a coherently-coupled two-level qubit. Tunnel coupling Ω and bare energy asymmetry $\delta \equiv \frac{1}{2}|E_1 - E_0|$ are defined in Fig. 11. (b,c) QAD qubit tunneling conductance calculated via the chiral Luttinger liquid theory for the $f = 1/3$ FQH fluid. All energies are in units of renormalized tunnel coupling $\tilde{\Omega}$; the asymmetry of coupling to the tunneling electrodes is $\alpha = \Gamma_0/\Gamma_1$. The coherently-split experimental peaks of unequal amplitudes (Fig. 8b) are evidence for $\delta \neq 0$ *and* $\alpha \neq 1$. [20]

2.4. *Theory work.* -- In addition to support of experimental work, Fig. 9, theoretical work focused on dynamics of LQP transport in FQH edges. This work is based on application of chiral Luttinger liquid (χLL) theory to coherent quasiparticle tunnel transport in constrictions and QAD's. More recently, these theoretical techniques have been applied to the experimental geometries and conditions, specifically to the double-QAD qubit weakly coupled to the electrode edges, Fig. 9. [20] A systematic investigation of small QAD arrays has been initiated, aimed at elucidating the designs favorable for protected logical qubits and the adiabatic ground-state quantum logic.

Antidot tunneling between quantum Hall liquids with different filling factors. We have developed a theory of quasiparticle backscattering in a system of point contacts formed between single-mode edges of several FHQ fluids with, in general, different filling factors f_j and one common single-mode edge f_0 of another FQH fluid. In the strong-tunneling limit, the model of quasiparticle backscattering is obtained by the duality transformation of the electron tunneling model. [36] We also considered tunneling through two point contacts between two edges of quantum Hall liquids of different filling factors $f_{0,1} = 1/(2\,m_{0,1} + 1)$ with $m_0 - m_1 = m > 0$. Properties of the antidot formed between the point contacts in the strong-tunneling limit are shown to be very different from the $f_0 = f_1$ case, and include the vanishing average total current in the two contacts and quasiparticles of charge e/m. For $m > 1$, quasiparticle tunneling leads to nontrivial m-state dynamics of effective flux through the antidot, which restores the regular "electron" periodicity of the current in flux, despite the fractional charge and statistics of quasiparticles. [37] These results exploit our earlier solution of a model of tunneling between a multichannel Fermi liquid reservoir and an

edge of the principal FQH fluids in the strong-coupling limit. The model explicitly takes into account quantum coherence of electrons in different reservoir channels, the fact that makes it important to determine their mutual exchange statistics. Our solution shows that the statistics is in general hyperfermionic, with the phase branches of the statistical factor -1 taking different values πx odd depending on the distance between the points of tunneling from the reservoir channels into the chiral edge. The choice of the statistics determines the saturated current between the edge and reservoir under non-vanishing bias voltage. If the tunneling points are well separated from one another, the outgoing edge is equilibrated with the reservoir as the number of reservoir channels is increased. The equilibration implies that the universal two-terminal conductance of the FQH edges is fractionally quantized, in contrast to a one-dimensional Tomonaga-Luttinger liquid wire, where a similar tunneling model predicts bare free-electron conductance. On the fundamental level, this difference is associated with the absence of time-reversal symmetry at high energies in the FQH case, as manifested in the chiral edge propagation. [38]

2.5. -- Three graduate students and two postdocs are or were supported (not concurrently) by this ARO grant. The ARO-supported work resulted in eight publications in refereed journals, Refs. 14, 15, 18, 24, 36-38 and two in refereed conference proceedings. Additionally, two manuscripts have been submitted (Refs. 25, 26), and two are in preparation (Ref. 20). This work also was basis of 19 scientific presentations (7 invited, three posted on web sites). The major results on direct observation of anyonic braiding statistics in a LQP interferometer reported in Refs. 14 and 15 were subject of a Physical Review Focus story [21], and several print and internet stories in US and international popular media, and various “journal club” presentations posted on the web.